EXPERIMENTALLY DETERMINED FLUTTER FROM
TWO- AND THREE-BLADED MODEL BEARINGLESS ROTORS IN HOVER

William G. Bousman and Seth Dawson
Research Scientists
U.S. Army Aeromechanics Laboratory — AVSCOM
Moffett Field, California 94035-1099

Abstract

A series of experiments was performed on a 1.8-m-diam model rotor in hover for the principal purpose of investigating the lead-lag stability of isolated bearingless rotors. Incidental to those tests, at least three types of pitch-flap flutter were encountered; those flutter types constitute the subject matter of this paper. Type 1 flutter occurred approximately at the second flap-mode frequency on both two- and three-bladed rotors for both small and large pitch angles and appeared to be a classic pitch-flap flutter. Type 2 flutter showed mostly torsional motion and was seen on both two- and three-bladed rotors. The flutter mode appeared to b the rotor first-torsional mode and the flutter occurred just above 3/rev for low pitch angles. This behavior is similar to wake-excited flutter, but the flutter mode was in the wrong sense for a flutter dependent on lining up of the shed wakes. Type 3 flutter was a regressing flap flutter that occurred for only the three-bladed rotor configurations and appears to be a wake-excited flutter. Although flutter occurred on a number of different configurations, no rotor parameters were identified that were clearly stabilizing or destabilizing.

Introduction

In the context in which it is used in this paper, flutter refers to instabilities that primarily involve pitching or flapping motions of a rotor blade and that are essentially unaffected by lead-lag motion. The analytical efforts of Loewy and of Miller and Ellis[2] have provided a good understanding of pitch-flap flutter of articulated rotors, and the general features have been confirmed by experiment.[3] Flutter can be prevented in general if the blades are quarter-chord balanced (which is important for control loads as well) and if the control system and blade torsional mode are made relatively stiff. Stability is degraded with a rearward shift of the center of gravity (c.g.) of the blade with respect to the aerodynamic center or if

the rotor torsional stiffness is reduced. For the most part, flutter has not caused major developmental problems with recent rotor designs, although the exceptions[4,5] have been remarkable in their complexity and belie the simple definition of flutter used here.

In the design of bearingless rotors in general and of bearingless tail rotors in particular, a number of flutter problems have been encountered that appear to be caused partly by the low torsional stiffness of those designs and partly by structural coupling. Development of the YUH-61A bearingless tail rotor revealed both flap-lag and flutter-type instabilities[6] that although eliminated during testing were never understood. Model tests of a similar configuration at Bell Helicopter exhibited a number of instabilities that showed flutter behavior.[7] It is not clear at the present time whether these recent problems are fundamentally more complex because of the structural coupling that is inherent in bearingless-rotor designs or that designers are simply working closer to flutter boundaries that have been there all along.

A recent series of experiments has been performed at the U.S. Army Aeromechanics Laboratory for the purpose of better understanding design parameters that will affect the lead-lag damping of an isolated bearingless rotor in hover. A number of different types of flutter were encountered in these tests, some of the results of which were presented in Ref. 8. Because the flutter encounters were incidental to the purpose of the tests, only limited data were acquired to characterize these cases. However, it is believed that sufficient data were obtained to provide a preliminary assessment of the flutter types that were encountered, and it is the purpose of this paper to provide that assessment. The series of experiments that has been run will be briefly described and the experimental procedures used when flutter was encountered will be described. The types of flutter that were encountered will be described and quantified, and some discussion will be provided on the sources of the flutter types and the effect of configuration.

Description of Experiments

A 1.8-m-diam bearingless rotor was tested in hover in both two-bladed and three-bladed configurations in a series of experiments. An overall view of the two-bladed model is shown in Fig. 1; the three-bladed model is shown in Fig. 2. Because identical blades and root hardware were used in all the experiments, the only difference between the two- and three-bladed configurations is the rotor solidity. Model properties are tabulated in the Appendix.

An exploded view of the flexbeam and root hardware for a single blade is shown in Fig. 3. The flexbeam has a uniform rectangular cross section along its length and is made of Kevlar fibers in an epoxy matrix. The flexbeam is fastened to the hub with a root socket that allows the flexbeam to be inclined at any pitch angle θ_f and a precone adapter that gives the flexbeam a precone angle β_f. The flexbeam is connected to the blade through the blade root fittings, the torque tube, and a plug socket that fits inside the torque tube. The blade can be pitched with respect to the flexbeam at the blade root fittings; the angle between the flexbeam and the blade is θ_b. The blade can be drooped either up or down (by an angle β_b) using an angled shim, and it can be swept (angle ζ_b) using a different shim. Two pitch links may be used as shown in the figure or a single pitch link may be installed on either the leading or trailing edges. The radial location of the pitch links may be changed to a number or intermediate positions between the flexbeam root and the flexbeam tip; this change in the location of the pitch links affects the pitch-flap coupling. The ends of the pitch links are small flexures that represent a frictionless rod end bearing that is very stiff axially, but very soft laterally. The blade pitch angle θ was set by raising or lowering the pitch links by hand, with the blade supported such that there was no flap deflection.

Initial testing of the three-bladed rotor configuration indicated that the determination of lead-lag damping was very sensitive to dissimilarities in the mass and stiffness of the blades. As a result, a major effort was made to make the blades and flexbeams as uniform as possible. To this end, 20 flexbeams were built and individually tested for stiffness by attaching a 0.63-kg weight to the plug socket and measuring the lead-lag frequencies. The flexbeams that showed the closest match were then modified by removing 0.001-0.002 in. of material, and a final set of matched flexbeams was obtained whose lead-lag frequencies were within 0.1% of each other. No attempt was made to match the flap frequencies. In a similar way, the blade inertias were tuned by adding tantalum weights to the blade tip at the quarter-chord location. The frequencies of the three-bladed test flexbeam/blade combinations following instrumentation and installation on the model matched within 0.3% for lead-lag and 0.4% for flap.

Each flexbeam was instrumented with strain-gage bridges to measure flap, lead-lag, and torsion bending moments. The signals were transferred from the rotating system, using a 40-channel slip ring for the two-bladed tests and a 65-channel slip ring for the three-bladed test. Fixed system instrumentation included a 1/rev pip, an accelerometer to measure the upper stand motion, and a clamp signal to indicate locking of the upper stand. The resulting data were digitized for on-line analysis and stored on disk; in most cases they were recorded on analog tape as well.

The same stand, drive system, and excitation system were used for the two- and three-bladed tests. The blades and hub were mounted to an upper stand that was free to pivot on flexures when unclamped and that was locked solidly with air clamps before data were taken. The normal procedure for obtaining lead-lag frequency and damping was to free the upper stand, oscillate the hub and stand at $\omega_\zeta + \Omega$ or at $\omega_\zeta - \Omega$ (where ω_ζ was the lead-lag frequency and Ω the rotor speed) with a shaker and, once sufficient lead-lag motion was obtained, to turn off the shaker and clamp the stand. The frequency and damping were obtained from the resulting transient decay using the moving-block analysis.

The design of the experiment did not consider the possibility that flutter might be encountered during testing, and therefore neither the experimental setup nor the on-line data analysis procedures were well-suited for an investigation of the various types of flutter that were encountered. The general procedure that was used when a flutter was encountered was to approach the flutter boundary in small increments of rotor speed, taking both digital records and analog tape records. Test points at which the rotor was unstable were recorded, unless the loads increased too quickly in which case the rotor speed was reduced to a stable condition. Considerable time was spent during the first flutter encounters in attempting to understand the character of the flutter. When it was thought that the flutter was caused by coupling of the second flap and first torsion modes, the upper stand was oscillated at the appropriate frequencies to excite those modes. This was a fairly successful technique for exciting the second flap mode, but it was ineffective in exciting the first torsion mode. This is not surprising, considering that the blades were quarter-chord balanced and could not be inertially excited with

hub shaking. A recording oscillograph was used for examining particular flutter occurrences and to infer the mode shape of the flutter and understand its behavior.

Unfortunately, these procedures were time consuming and detracted from the original objectives of the experiments. As additional flutter incidents were encountered, less effort was expended on documenting the flutter; this was particularly so if the flutter appeared to be similar to that observed in a previous encounter. At the start of the three-bladed tests, a systematic effort was made to avoid configurations that had produced flutter in the two-bladed tests. This approach was effective in maximizing the use of available test time, but did not develop the data that would allow a better understanding of the flutter incidents that had been examined in the two-bladed tests.

Data Analysis Procedures

The run logs from various experiments with the bearingless-rotor models were examined, and test points were selected at which a flutter was encountered. In addition, supplemental test points were chosen for stable conditions that were proximate in rotor speed or pitch angle to the flutter conditions. Approximately 170 cases for 13 different configurations were selected for flutter analysis.

The data recorded on analog tape were sampled at 800 Hz to provide an ample bandwidth for analysis and time-histories with good resolution. The flexbeam strain-gage bending-moment data were converted to angular deflections at the flexbeam tip to provide a basis of comparison for the flap, lead-lag, and torsion motions. The conversion used static calibration factors and, therefore, introduced some error in that the effect of the centrifugal force on the bending-mode shape was ignored. However, those errors are not considered important to obtaining a better understanding of the model rotor flutter characteristics. For each case, approximately 5 sec of data were obtained and the time-histories were examined for unstable behavior. The frequency spectrum of an appropriate coordinate was examined to determine what modes were involved, and damping was estimated using the moving-block analysis. Vector plots were obtained at the appropriate modal frequencies to determine the amplitude and phase of the modal behavior in the physical coordinates.

Description of Types of Flutter

Twenty-eight different combinations of rotor configuration, blade number, and pitch-link radial location were tested during this series of experiments; they are described in Table 1. Of the 28 combinations there were 3 in which pitch links were installed on both the leading and trailing edges [designated (1a), (6a), and (6c)]. This simulates a vertical shear restraint at the root of the blade and substantially increases the torsional stiffness of the rotor to above 10/rev. No indication of flutter was ever noted for these torsionally stiff, two-pitch-link cases. Of the remainder of the combinations tabulated, the run logs indicated that flutter was encountered on 15 of the 28. However, following the analysis of all potential flutter cases some form of flutter was seen and documented for 12 of the cases in Table 1. (Of the three undocumented cases, two appear to have been a flutter, and the other a 3/rev response.) The flutters encountered appear to fall into three general categories, as shown in Fig. 4. Type 1 flutter occurred at rotor frequencies between 2/rev and 3/rev and was seen for both two- and three-bladed rotor configurations. It appears that it occurred at all pitch angles, although most of the records are for a pitch angle of 0°. Substantial flap and torsion motions of the blade were involved in all cases, and the unstable modal frequency was near the expected second flap mode frequency. In this sense, the Type 1 flutter appears much like a classic pitch-flap flutter.

Type 2 flutter was also encountered on both the two- and three-bladed configurations, but at frequencies above 3/rev. In all cases, the flutter appeared to occur at the first torsion-mode frequency, and the modal content was almost purely torsion. This flutter could only be found at pitch angles of 0° and 2°, which suggests that coupling with the wake is important. Neutral stability or limit-cycle behavior was observed over a range of rotor speeds rather than at a specific stability boundary.

Type 3 flutter was a regressing flap-torsion flutter that occurred just above 1/rev. It was found only for the three-bladed configurations and only at a pitch angle of 0°. It occurred over a broad range of rotor speeds and, as with the Type 2 flutter, it appears to be related to the wake.

Type 1 Flutter

Flutter that was classified as Type 1 occurred on four configurations [(2a), (2b), (2c) (two blades); and (17a) (three blades)]. [Hereinafter, the rotor configurations will be referred to by their number and letter designators – e.g., (3a), (14c).] An

example of a Type 1 flutter for (2c) is shown in Fig. 5 which shows a segment of the flutter time-history and a vector phase plot. From this figure it can be seen that the flutter mode shows approximately the same flap and torsion deflections and that for each blade the flap and torsion motion is out of phase. Looking at the time-history, the motion between blades appears to be approximately in-phase and, hence, a collective motion; this is quantified on the vector plot which shows that blade 1 leads blade 2 by about 40°.

An example of a flutter point for each of these configurations [(2a), (2b), (2c), and 17a)] is given in Table 2 which shows the parameters that characterize the configuration; the pitch angle θ and the rotor speed Ω of the flutter point; and the modal frequency ω, damping σ, and mode shape. Note that the first line of the mode shape refers to the modal amplitude for blade 1, the second line for blade 2 and so forth. For (2c), unstable or neutrally stable conditions existed over rotor speeds from 700 to 742 rpm at a blade pitch angle of 0°; this is indicated in Table 2 by showing both the low and high ends of the rotor speed range. Also note that there is no lead-lag motion for any of the Type 1 flutter points. All the Type 1 flutters encountered with two blades and at 0° showed an approximate in-phase behavior, with blade 1 leading blade 2 by 5°±5° for (2a) (mean±standard deviation, sample of 7); by 13°±9° for (2b) (sample of 10)/ and by 39°±4° for (2c) (sample of 7). However, different phase behavior was seen for (2c) at a pitch angle of 6° and for (17a), as is discussed below.

Configurations (2a), (2b), and (2c) were made except for the radial location of the pitch link on the leading edge. The major effect of this change in pitch-link location is a change in the pitch-flap coupling. At the inboard location, the pitch-flap coupling is positive with more amplitude in flap than pitch for the first flap mode under nonrotating conditions. For (2b), with the pitch link located radially at about the midspan of the flex-beam, the pitch-flap coupling is zero. In the outboard location [configuration (2c)] the pitch-flap coupling is negative. The effects of these differences on the predicted modal frequencies is shown in Fig. 6 which is taken from Ref. 8. These predictions were made using the FLAIR analysis.[9] The flutter-mode frequencies have been added to this figure; they indicate the approximate location of the second flap mode which is not predicted by the FLAIR analysis. As the predicted frequencies show, the major effect of the differences in pitch-flap coupling is on the location of the first-flap-mode frequency; little

effect is seen on the torsion frequency. As is shown in Table 2, the effect of pitch-flap coupling is to shift the initial flutter point to higher rotor speeds; that is, the flutter point is 700 rpm for negative pitch-flap coupling, 980 rpm for no pitch-flap coupling, and 1100 rpm for positive pitch-flap coupling. Despite this shift in the flutter point, the basic character of the flutter is unchanged; that is, the flap and torsion motions are out-of-phase regardless of the pitch-flap coupling.

A closer examination of the (2c) flutter encounters raises some additional questions about the cause of this flutter and suggests that the situation may be more complex than it first appears. Figure 7 characterizes the flutter behavior for pitch angles of 0° and 8°. At 0°, the modal damping is essentially neutral from 700 to 750 rpm. It is not until the 762-rpm point is reached that the flutter shows substantial unstable behavior. However, at each higher rotor speed the modal amplitude increases. This suggests that over the initial rotor-speed range the flutter is showing limit-cycle behavior, and it is not until 762 rpm that the destabilizing effects are sufficient to cause a normal exponential instability. It is also possible that even the 762-rpm point would have eventually shown limit-cycle behavior if it had not been necessary to shut down the rotor because of excessive loads. At 8°, a different flutter behavior is seen in that the damping changes rapidly from negative to positive values in a classic stability boundary fashion, and there is no sign of limit-cycle behavior. More interesting, still, the behavior of the flutter changes from an apparent collective second-flap mode to a differential second-flap mode (see Table 2).

The data analysis program is able to examine the flutter condition in either conventional blade coordinates (as in Fig. 5) or in multiblade coordinates. For the two-bladed rotor, the flapping multiblade coordinates are simply collective and differential coordinates, and they allow collective and differential behavior to be more easily observed. For the 8° case, two frequencies were evident and they appeared primarily in either the collective or differential coordinates. Where a lightly damped or unstable condition was observed it was always the differential mode. The collective mode appeared to be stable for these conditions, but because of its proximity to the differential mode, no acceptable estimate of its damping could be made. In the 0° case, only a collective-mode behavior was observed with no sign of a differential mode. In interpreting these differences, however, it is necessary to recognize that the blade second-flap-mode frequencies are not known to be identical and that a two-bladed rotor with dissimilar properties can

show apparent collective- and differential-mode behavior that may not be representative of rotors with identical properties. In addition, even though the collective mode is uncoupled from the stand, the differential mode will appear in the fixed system at about 50 Hz and may couple with the first stand mode, which has a frequency of 77 Hz. Further investigation is required to understand the different behavior of the collective and differential modes.

Flutter boundaries were noted at other pitch angles for (2c) in the run logs, both in the two- and three-bladed tests, but no other unstable conditions were recorded on analog tape. For (2a) and (2b), flutter was not encountered at pitch angles away from 0° within the rotor speed limits of the model.

A flutter or near-flutter case was documented for a three-bladed configuration [(17a)] that was classified as a Type 1 flutter on the basis of the modal frequency. However, in other respects this flutter case appears different from those that have been discussed so far. A segment of the time-history and the vector plot are shown in Fig. 8. Unfortunately, two of the three flapping bridges have failed (this was the last configuration tested), and the behavior must be deduced from the remaining flapping bridge and the three torsion bridges. The torsion amplitude is greater than the flap amplitude in this case and, where the previous zero pitch angle cases showed that instability was essentially a collective mode (both blades in phase), the apparent mode here is a progressing or forward whirling mode. These differences suggest a different type of flutter behavior or mechanism, but the lack of additional flutter data makes this unclear.

Type 2 Flutter

Flutter that was classified as Type 2 occurred on four combinations [(3a) (three blades); and (3a), (4a), and (5a) (two blades)]. A sample time-history and its associated vector phase plot for (3a) are shown in Fig. 9. Unlike the Type 1 flutter, which was characterized by significant amounts of flap and torsion motion, this case shows essentially all torsion motion. The flutter frequency occurs at the first-torsion-mode frequency which is slightly above 3/rev. The time-history and phase plot show that the blade motions are essentially in phase, with blade 1 leading blade 2 by 38°, hence a collective torsion flutter.

Sample flutter points are given in Table 3 for each of these configurations. As before, when flutter was observed over a range of rotor speeds, both the low and high rotor speed are shown. For (3a),

blade 2 lags blade 1 by 39°±3° (sample of 11). For (4a) and (5a), amplitude and phase information are not shown because of signal calibration problems, but the phase angles, which were unaffected by the calibration problems, showed blade 2 lagged blade 1 with phase angles from -1° to 33°. As with Type 1 flutter, no lead-lag motion is observed at the flutter frequency. Unlike the Type 1 flutter cases, however, Type 2 flutter was only seen for the inboard, trailing-edge pitch-link position, which results in negative pitch-flap coupling. The difference between the three configurations in this case was the presence or absence of flexbeam or blade precone, and this seems to have had only a minor effect on the occurrence of Type 2 flutter.

Flutter was encountered on (3a) over a wide range of rotor speeds and for both the two- and three-bladed cases. Figure 10 shows the frequencies calculated with FLAIR for this configuration.[8] The flutter frequencies have been added to this figure, and it can be seen that they agree very well with the predicted first-torsion frequency. The flutter encountered with (3a) is further described in Fig. 11, which shows the modal amplitudes, damping, and frequencies for both the two- and three-bladed tests. For the range of rotor speeds over which the flutter was examined, the rotor showed neutral stability or limit-cycle behavior. However, as rotor speed increased, the modal amplitude increased as well. That this is related to the flutter and not just a response to 3/rev excitation is shown by the plot of the 3/rev response in torsion, which does not change noticeably over the range of rotor speeds investigated. As shown in Table 3, the two-bladed Type 2 flutter is mostly torsion amplitude, with the two blades nearly in phase. For the three-bladed case, this behavior is changed, as shown in Fig. 12 in which the vector phase plots are compared. Although blades 1 and 3 are not far apart in phase, blade 2 is of opposite phase. There is significantly more blade flapping now than was seen in the two-bladed case. (Note that if a response in a degree of freedom is less than 10% of the largest component, it is not shown in these vector phase plots.) Unlike the two-bladed case in which the phase relation was invariant with rotor speed, substantial differences were seen for the three-bladed rotor for different rotor speeds as indicated in Table 3.

Configurations (4a) and (5a) were tested at a pitch angle of 2° (the normal increment in pitch angle was 4°); they too showed the Type 2 flutter. However, no incidence of flutter was documented for any configuration at larger pitch angles. This absence of flutter at higher pitch angles

suggests that the flutter is related to the wake and is perhaps wake-excited.

Type 3 Flutter

Type 3 flutter was encountered on four three-bladed configurations [(7c), (14c), (15a), and (16a)]. An example is provided in Fig. 13 for (15a). The sample time-history shows a low-frequency flutter that is only slightly above 1/rev. For each blade, the flap and torsion motions are in phase, with flapping roughly twice the magnitude of torsion. Blade 3 lags the motion of blade 2, which in turn lags blade 1; this represents a regressing or backward whirl mode if viewed in the fixed system. Figure 13 gives the appearance of a coupled flap-torsion flutter; however, the flapping mode at this frequency appears in both flap and pitch coordinates, and because of the positive pitch-flap coupling the motion appears in phase. Thus, it appears that the Type 3 flutter is a single-degree-of-freedom flutter, as was seen for Type 2.

Sample flutter points are provided in Table 4 for the various Type 3 flutter cases. Except for (16a), the flutter was encountered over a range of rotor speeds and it gave the appearance of neutrally stable or limit-cycle behavior. For all configurations tested, the mode shape was the same with the blade flap and torsion in phase and a 120° phase difference between the blades. Note that as in the other flutter cases, there is no motion in the lead-lag coordinate.

More detailed information on the Type 3 flutter is provided in Fig. 14 for (7c) and (14c). These configurations differ only in the addition of a boundary-layer trip to the outer 5 in. of each blade on the upper surface at the 25% chord location. The trip used a 1/16-diam twine that was glued on. The trip was added to see if boundary-layer disturbances could significantly affect the observed flutter behavior, as has occurred in previous model investigations.[10] Configurations (7c) and (14c) show essentially identical behavior, and, although the rotor-speed range for neutral or limit-cycle behavior is shifted to higher rotor speeds for (14c), the use of the trip does not eliminate the flutter. Both configurations show a relatively wide range of limit-cycle or unstable behavior, with the amplitude increasing as rotor speed increases. No flutter was encountered for these configurations for pitch angles of ±4°, which suggests that the flutter is wake-coupled – behavior similar to that seen in the Type 2 flutter cases.

Discussion

Wake-Excited Flutter

At low blade-pitch angles and induced velocities in hover, the spacing between the shed wakes can become quite small, and, if the frequency of an oscillation is such that the shed wakes reinforce each other, a flutter can occur that is termed wake-excited flutter. It often appears as a single-degree-of-freedom flutter. Wake-excited flutter may occur for a single blade or for a rotor with any number of blades. In the latter case, the actual frequency will depend on the particular mode of the rotor that is involved. Anderson and Watts[4] provide a good discussion of how the wakes will line up for the various modes of a four-bladed rotor. The same principles can be applied for the two- and three-blade rotors that were tested in the experiments reported here. Depending on the blade mode involved, a particular frequency ratio ω/Ω will result in the shed wakes, reinforcing and causing a wake-excited flutter. The frequency ratios for potential wake-excited flutter for two- and three-bladed rotors are shown in Table 5. If, for an example, a blade torsion mode or flap mode is near a 4/rev resonance with rotor speed, then there is a potential for a wake-excited flutter in the collective mode for a two-bladed rotor or for the cyclic regressing mode for a three-bladed rotor. With the use of this table it is possible to examine the experimentally determined flutters that occurred near per-rev crossings and determine if they can be categorized as wake-excited flutter.

The Type 2 flutter was essentially a pure torsion flutter, and it occurred on both two- and three-bladed rotor configurations near the 3/rev crossing of the first torsion mode; it was not observed at pitch angles greater than 2°. In this sense, the flutter acts like a classic wake-excited flutter. From Table 5 it can be seen that a wake-excited flutter at 3/rev should occur in the differential mode for a two-bladed rotor and in the collective mode for a three-bladed rotor. However, the experimentally determined flutter mode is close to a collective mode for all the two-bladed encounters whereas for the three-bladed case no fixed system mode could be defined. This suggests that the Type 2 flutter is not wake-excited in the classic sense of a flutter induced from reinforcement of previous wakes.

The Type 3 flutter appeared close to a 1/rev crossing near the first-flapping-mode frequency and was not observed away from a pitch angle of 0°. It occurred only for the three-bladed rotor configurations. From Table 5, a 1/rev wake-excited flutter should occur only for the regressing

74

mode of a three-bladed rotor, and this is what was seen in the experimental measurements for all four configurations in which this type of flutter was encountered. In this case, then, it seems clear that the Type 3 flutter is wake-excited and occurs because the first flap mode is crossing the 1/rev because of positive pitch-flap coupling.

In some cases, the Type 1 flutter encounters showed behavior that appeared as though they might be related to wake reinforcement, although in no cases were the flutter frequencies as close to a per-rev crossing as in the Type 2 and Type 3 encounters. However, it may be useful to look upon Table 5 as a means by which the Type 1 flutter encounters might be better understood. For (2c), the Type 1 flutter showed limit-cycle behavior over a range from 700 to 750 rpm. The flutter mode frequency in this case ranged from 2.8/rev to 2.7/rev. This would suggest an excitation of the second flap mode by the coalescence of wakes at 3/rev; however, from Table 5 this should occur only in a differential mode, whereas experimentally the observed mode was a collective one. For (17a), the observed mode was largely a torsion response at 2.4/rev, and from Table 5 for a three-bladed rotor this suggests excitation of the second flap mode by 2/rev wake reinforcement, which should occur in a progressing mode. Interestingly enough, this is what was seen in the measurements, although the lack of additional experimental cases for (17a) makes any conclusions impossible.

Effect of Configuration

As shown in Table 1, 28 different configurations, blade numbers, and pitch-link radial locations were tested and only 12 showed a documented case of flutter. In looking at those cases that had flutter and those that were flutter-free, it may be asked if there are any definite conclusions that can be made about the effect of configuration. Clearly the configurations with two pitch links were without flutter, but this is not surprising, considering that the torsional stiffness was above 10/rev. The Type 1 flutter configurations seemed to show the largest variation in parameters, with no particular parameter obviously dominant. This flutter occurred for pitch-flap coupling of approximately -0.5, 0, and +0.5, with the pitch link on the leading edge, but in none of the cases with the pitch link on the trailing edge. The least stable configuration was (2c), with the pitch link on the leading edge and negative pitch-flap coupling. Because this configuration was purposely avoided in subsequent tests, it is difficult to determine if these results were in any sense typical.

The Type 2 flutter cases all had negative pitch-flap coupling, and the only other two-bladed configuration with negative pitch-flap coupling that did not show Type 2 behavior was (2c), which went unstable at a lower rotor speed with Type 1 flutter. Of the three-bladed configurations with negative pitch-flap coupling that were tested, one showed Type 2 flutter, but the other two did not.

Type 3 flutter occurred only for three-bladed rotor configurations with positive pitch-flap coupling. However, these cases included configurations with droop, precone, sweep, and the pitch link on either edge. Similar configurations with positive pitch-flap coupling showed no instability. The absence of an obvious dependency of a specific flutter type on configuration suggests that future design must continue to be guided by detailed analysis and model test.

Conclusions

A number of different flutter types were encountered in a series of experiments undertaken to determine the lead-lag stability in hover of a bearingless rotor mounted on a rigid hub. These flutter cases have been analyzed and the following conclusions made.

1) Three distinct types of flutter were encountered that may be separated on the basis of the flutter mode frequency. a) A flutter mode that occurs at a frequency between 2/rev and 3/rev which corresponds to the model rotor's second flap mode (Type 1); this flutter was seen on both two- and three-bladed rotors and showed significant flap and torsion motions. b) A flutter mode that occurs at a frequency above 3/rev and corresponds to the model rotor's first torsion mode (Type 2); this flutter mode was seen on both two- and three-bladed rotors, and the motion was mostly torsion with very little flapping. And c) a flutter mode that occurs at a frequency close to 1/rev and is a regressing mode when seen in the fixed system (Type 3); this occurred only for three-bladed rotors.

2) Type 1 flutter was observed at pitch angles greater than 0° for the best documented configuration and in this sense represents a classic flap-torsion flutter that is not directly dependent on unsteady wake effects.

3) Type 2 flutter was observed on four configurations at pitch angles at 0° and 2°, but not at higher pitch angles. Its occurrence near the 3/rev crossing at low pitch angles suggests the flutter is wake-excited; however, it occurs in a collective mode rather than a differential mode for th :

two-bladed tests, and it does not appear in any clearly defined rotor mode in the three-bladed tests.

4) Type 3 flutter was observed on four configurations at a pitch angle of zero degrees, but not at higher pitch angles. It appeared only for three-bladed configurations in a regressing mode near the 1/rev crossing which corresponds to the expected mode of instability for a wake-excited flutter.

5) The effects of rotor configuration on the various forms of flutter were examined, but there were no configuration parameters that were clearly stabilizing or destabilizing for torsion-mode frequencies below 10/rev.

Appendix: Model Properties

The model rotor geometric properties are shown in Table 6. Rotor mass properties are given in Table 7. The blade mass is concentrated in the torque tube and root hardware, which are not representative of that of a full-scale rotor. The center of gravity of the blades alone was determined from measurements on four blades; it was located at 26.2% chord with a range of values from 25.6% to 26.6%. If the chordwise c.g. of the combined blade and root hardware is considered, the c.g. is shifted to 25.1% chord because of the mass of the root hardware. This does not adequately represent the cross-product term of c.g. offset with radius, which is important for flutter calculations; however, no estimate was made of an equivalent c.g. based on the correct cross-product term. Measurements were made of nonrotating frequencies of the blades both with and without pitch links; these are provided in Table 8. The measurements with the pitch link installed are for (3a), that is, the pitch link is located on the trailing edge at the inboard location. The nonrotating frequencies for other configurations do not differ significantly from the tabulated values in Table 8. Nonrotating measurements were made of the pitch-flap coupling for a few configurations and the values ranged from +0.41 to +0.49 for four configurations, with the pitch link at the inboard position on the trailing edge. (Comparable values of negative pitch-flap coupling have not been obtained.) The blade airfoil section of the model is a NACA 23012.

References

1. Loewy, Robert G., "A Two-Dimensional Approximation to the Unsteady Aerodynamics of Rotary Wings," Journal of the Aeronautical Sciences, Vol. 24, Feb. 1957, pp. 81-92, 144.

2. Miller, R.H. and Ellis, C.W., "Helicopter Blade Vibration and Flutter," Journal of the American Helicopter Society, Vol. 1, No. 4, July 1956, pp. 19-38.

3. Daughaday, Hamilton, DuWaldt, Frank, and Gates, Charles, "Investigation of Helicopter Blade Flutter and Load Amplification Problems," Journal of the American Helicopter Society, Vol. 2, No. 3, July 1957, pp. 27-45.

4. Anderson, William D. and Watts, George A.. "Rotor Blade Wake Flutter — A Comparison of Theory and Experiment," Journal of the American Helicopter Society, Vol. 21, No. 2, Apr. 1976, pp. 32-43.

5. Neff, James R., "Pitch-Flap-Lag Instability of Elastic Modes of an Articulated Rotor Blade," Proceedings of the 40th Annual National Forum, May 1984, pp. 573-579.

6. Shaw, John and Edwards, W. Thomas, "The YUH-61A Tail Rotor: Development of a Stiff Inplane Bearingless Flexstrap Design," Journal of the American Helicopter Society, Vol. 23, No. 2, Apr. 1978, pp. 9-18.

7. Harvey, K.W., "Aeroelastic Analysis of a Bearingless Rotor," American Helicopter Society Symposium on Rotor Technology, Aug. 1976.

8. Dawson, Seth, "An Experimental Investigation of a Bearingless Model Rotor in Hover," Journal of the American Helicopter Society, Vol. 28, No. 4, Oct. 1983, pp. 29-34.

9. Hodges, Dewey H., "An Aeromechanical Stability Analysis for Bearingless Rotor Helicopters," Journal of the American Helicopter Society, Vol. 24, No. 1, Jan. 1979, pp. 2-9.

10. Tinman, R. and van de Vooren, A. I., "Flutter of a Helicopter Rotor Rotating in Its Own Wake," Journal of the Aeronautical Sciences, Vol. 24, July 1957, pp. 694-702.

Table 1. Bearingless model rotor configurations

Configuration	Number of blades	Pitch-link position	Radial location[a]	θ_β[b]	θ_f, deg	θ_b, deg	β_f, deg	β_b, deg	ζ_b, deg	Flutter type
1a	2	LE/TE	10	0	0	0	0	0	0	None
2a	2	LE	10	+	0	0	0	0	0	1
2a	3	LE	10	+	0	0	0	0	0	None
2b	2	LE	50	0	0	0	0	0	0	1
2c	2	LE	90	-	0	0	0	0	0	1
2c	3	LE	90	-	0	0	0	0	0	(c)
3a	2	TE	10	-	0	0	0	0	0	2
3a	3	TE	10	-	0	0	0	0	0	2
3b	2	TE	50	0	0	0	0	0	0	None
3c	2	TE	90	+	0	0	0	0	0	None
3c	3	TE	90	+	0	0	0	0	0	None
4a	2	TE	10	-	0	0	2.5	0	0	2
5a	2	TE	10	-	0	0	0	2.5	0	2
6a	3	LE/TE	10	0	0	0	0	0	-2.5	None
6c	3	LE/TE	90	0	0	0	0	0	-2.5	None
7a	3	TE	10	-	0	0	0	0	-2.5	None
7c	3	TE	90	+	0	0	0	0	-2.5	3
8a	3	LE	10	+	0	0	0	0	-2.5	None
8c	3	LE	90	-	0	0	0	0	-2.5	(c)
9a	3	LE	10	+	0	0	0	2.5	-2.5	None
10c	3	TE	90	+	0	0	0	2.5	-2.5	None
11a	3	LE	10	+	0	0	2.5	0	-2.5	None
12a	3	LE	10	+	0	8	0	0	0	None
13a	3	LE	10	+	-8	8	0	0	0	None
14c[d]	3	TE	90	+	0	0	0	0	-2.5	3
15a	3	LE	10	+	0	0	2.5	0	0	3
16a	3	LE	10	+	0	0	0	2.5	0	3
17a	3	LE	10	+	0	8	0	0	-2.5	1

NOTE: Symbols are defined in text. Abbreviations in pitch-link-position column refer to leading and trailing edges.

[a] Percent of flexbeam length from flexbeam root.

[b] Pitch-flap coupling, positive pitch-flap coupling is flap up, nose up.

[c] Type 1 instability noted in run logs, but no documented record.

[d] Same configuration as (7c) except with boundary-layer trip on top surface.

Table 2. Type 1 flutter cases[a]

Configuration	Pitch-link position	Number of blades	θ_f, deg	β_b, deg	θ, deg	Ω, rpm	ω, Hz	σ, 1/sec	Mode Shape[b]					
									Flap		Chord		Torsion	
									Amplitude deg	Phase deg	Amplitude deg	Phase deg	Amplitude deg	Phase deg
2a	LE, inboard	2	0	0	0	1100	43.77	+0.30	0.22	0	0.01	-8	0.18	174
									0.16	5	0.00	-53	0.13	-178
2b	LE, center	2	0	0	0	980	40.17	-0.05	0.72	0	0.03	-12	0.69	178
									0.46	18	0.01	-131	(c)	(c)
2b	LE, center	2	0	0	0	1011	40.72	+0.64	0.87	0	0.04	-11	0.84	178
									0.55	17	0.01	-135	(c)	(c)
2c	LE, outboard	2	0	0	0	700	32.85	-0.00	0.84	0	0.02	-34	0.92	179
									0.42	42	0.02	-124	1.44	-137
2c	LE, outboard	2	0	0	0	762	33.44	+0 35	1.68	0	0.05	-36	1.96	-179
									1.30	35	0.06	-120	1.41	-145
2c	LE, outboard	2	0	0	8	889	33.97	+0.87	1.06	0	0.04	-137	1.45	-178
									2.56	-160	0.26	10	3.34	18
7a	LE, inboard	3	8	-2.5	0	999	39.96	-0.41	(c)	(c)	0.01	155	0.12	0
									(c)	(c)	0.01	62	0.23	-118
									0.08	136	0.02	-78	0.30	109

[a]All configurations have zero flexbeam and blade precone.

[b]Values in first horizontal line for each configuration are for blade 1; those in second line are for blade 2; those in third line are for blade 3.

[c]Failed strain gage.

Table 3. Type 2 flutter cases[a]

Configuration	Number of blades	β_f, deg	β_b, deg	θ, deg	Ω, rpm	ω, Hz	σ, 1/sec	Mode Shape[b]					
								Flap		Chord		Torsion	
								Amplitude deg	Phase deg	Amplitude deg	Phase deg	Amplitude deg	Phase deg
3a	2	0	ι	0	851	47.57	+0.02	0.04	-8	0.01	170	0.51	0
								(c)	(c)	0.03	44	1.06	36
3a	2	0	0	0	936	48.82	+0.27	0.02	-91	0.03	172	2.33	0
								(c)	(c)	0.05	54	2.08	38
3a	-	0	0	0	804	46.71	+0.02	0.06	-159	0.01	12	0.46	0
								0	102	0.00	100	0.19	-79
								0.12	-12	0.00	125	0.69	166
3a	3	0	0	0	900	47.33	+0.33	0.03	-155	0.01	3	0.35	0
								0.13	-11	0.01	11	0.26	-178
								0.06	-166	0.01	16	0.27	-42
4a	2	2.5	0	0	878	47.31	+0.98	-	-	-	-	-	-
								-	-	-	-	-	-
4a	2	2.5	0	2	940	47.95	+0.5	-	-	-	-	-	-
								-	-	-	-	-	-
5a	2	0	2.5	0	883	47.67	0.00	-	-	-	-	-	-
								-	-	-	-	-	-
5a	2	0	2.5	2	89f	48.14	+0.10	-	-	-	-	-	-

[a]All configurations have the pitch link at the inboard location on the trailing edge and are without flexbeam pitch or blade sweep.

[b]Values in first horizontal line for each configuration are for blade 1; those in second line are for blade 2; those in third line are for blade 3.

[c]Failed strain gage.

Table 4. Type 3 flutter cases[a]

Configuration	Pitch-link position	β_f, deg	δ_b, deg	ζ_b, deg	θ, deg	Ω, rpm	ω, Hz	σ, 1/sec	Flap Ampli-tude deg	Flap Phase deg	Chord Ampli-tude deg	Chord Phase deg	Torsion Ampli-tude deg	Torsion Phase deg
7c	TE outboard	0	0	-2.5	0	302	5.70	+0.08	0.51	0	0.01	166	0.29	0
									0.56	122	0.01	-71	0.29	122
									0.56	-121	0.00	-5	0.34	-116
7c	TE outboard	0	0	-2.5	0	407	7.30	+0.50	0.73	0	0.01	132	0.43	1
									0.68	127	0.01	-8	0.35	126
									0.91	-118	0.01	68	0.58	-120
14c[c]	TE, outboard	0	0	-2.5	0	401	7.20	-0.16	0.55	'	0.01	156	0.33	1
									0.50	12	0.01	-49	0.11	126
									0.58	-11t	0.01	68	0.36	-115
14c[c]	TE, outboard	0	0	-2.5	0	603	10.41	-0.02	0.93	0	t	148	0.60	1
									0.85	123	0.06	-98	0.20	123
									0.73	-118	0.01	157	0.49	-118
15a	LE, inboard	0	2.5	0	0	402	7.25	+0.02	0.30	0	0.01	-134	0.13	-9
									0.32	129	0.01	64	0.14	129
									0.54	-122	0.01	-29	0.26	-122
15a	LE, inboard	0	2.5	0	0	451	7.94	+0.09	1.20	0	0.02	-158	0.54	-8
									1.27	124	0.02	-30	0.55	125
									1.52	-121	0.01	-104	0.73	-120
16a	LE,	2.5	0	0	0	402	7.12	+0.05	0.13	0	0.00	-79	0.06	8
									0.13	122	0.01	2	0.06	123
									0.12	-121	0.00	-21	0.06	-120

[a]All configurations have three blades, no flexbeam pitch, and the pitch link locations result in positive pitch flap coupling.

[b]Values in first horizontal line for each configuration are for blade 1; those in second line are for blade 2; those in third line are for blade 3.

[c]Trip strip added to outer portion of blades.

Table 5. Frequency ratios for wake-excited flutter

ω/Ω	2-Bladed collective	2-Bladed differential	3-Bladed collective	3-Bladed regressing	3-Bladed progressing
1	---	X	---	X	---
2	X	---	---	---	X
3	---	X	X	---	---
4	X	---	---	X	---
5	---	X	---	---	X
6	X	---	X	---	---

Table 6. Rotor geometric properties

Property	Value
Radius, m	0.902
Blade chord, m	0.0419
Solidity per blade	0.0148
Flexbeam length, m	0.1016
Flexbeam width, m	0.00813
Flexbeam thickness, m	0.00361
Flexbeam tip distance from center, m	0.1782

Table 7. Rotor mass properties

Property	Blade/torque-tube	Blade
Blade mass, kg	0.460	0.102
Blade spanwise c.g., % radius	27.6	56.7
Blade chordwise c.g., % chord from leading edge	25.1	26.2
Blade flapping inertia about flexbeam center, $kg \cdot m^2$	0.02358	-
Blade pitch inertia, $kg \cdot m^2$	1.59×10^{-4}	-
Lock number	8.26	-

Table 8. Blade nonrotating frequencies[a]

Blade mode	Modal frequency (pitch link installed), Hz	Modal frequency (no pitch link installed), Hz
First flap	4.88	4.69
Second flap	24.81	24.81
First lead-lag	11.13	10.94
First torsion	38.28	19.73

[a]Measurements made on isolated blade of (3a).

Figure 1. Two-bladed bearingless-rotor model.

Figure 2. Three-bladed bearingless-rotor model.
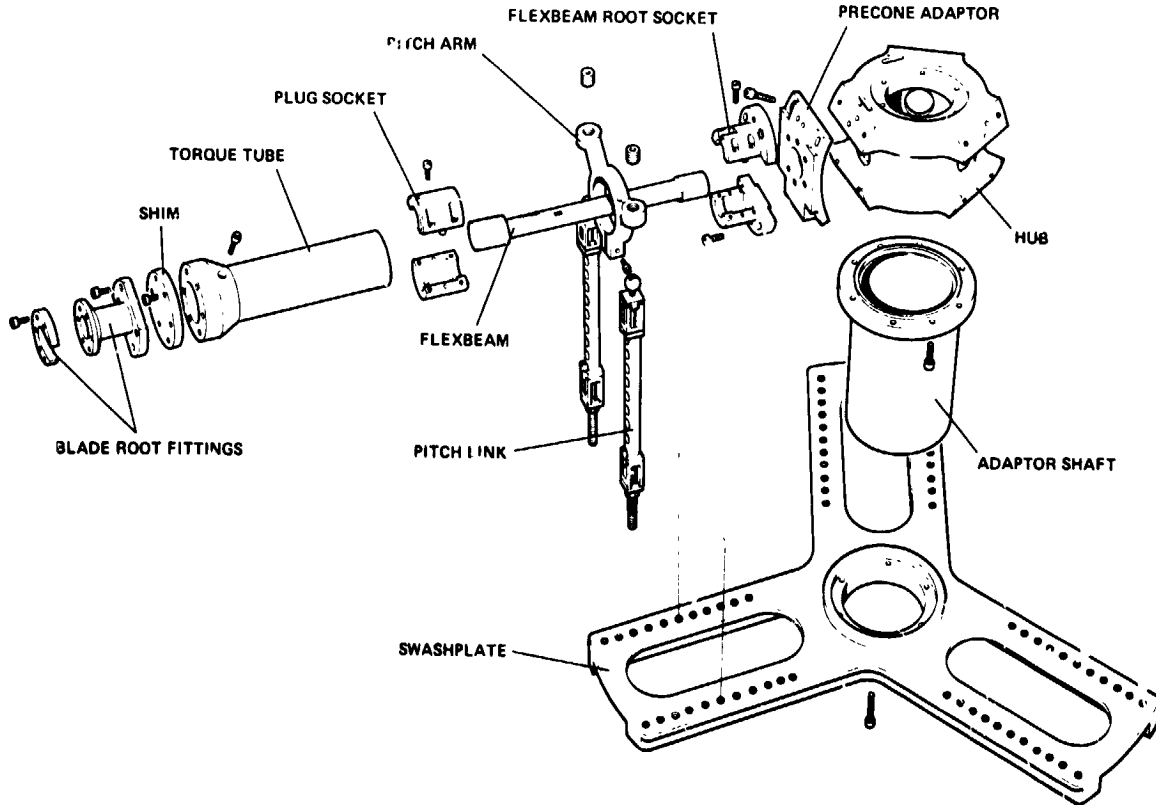
Figure 3. Exploded view of flexbeam and blade-root hardware.
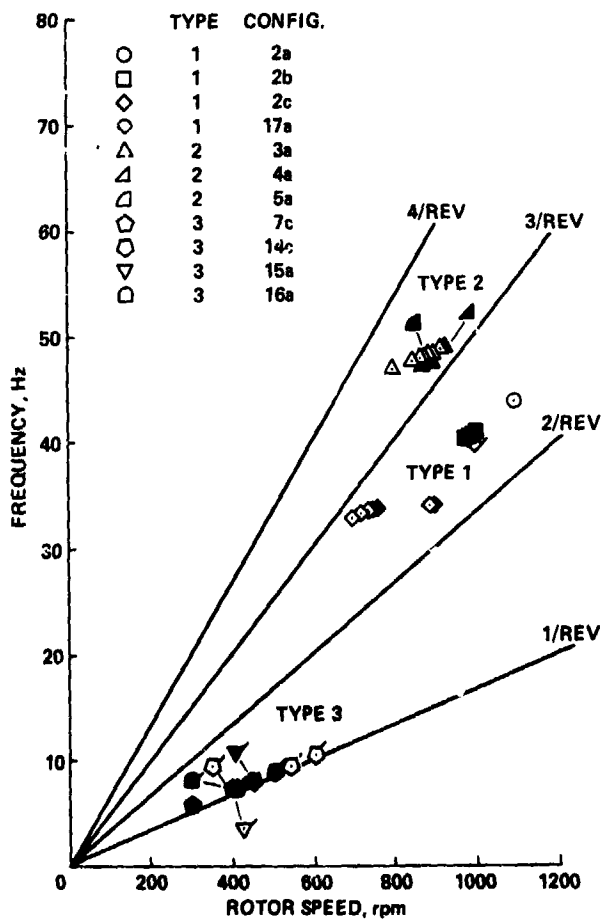
Figure 4. Frequency diagram showing types of flutter encountered. Open symbols are neutral stability points; closed symbols are unstable points; flagged symbols are for three-bladed rotor.
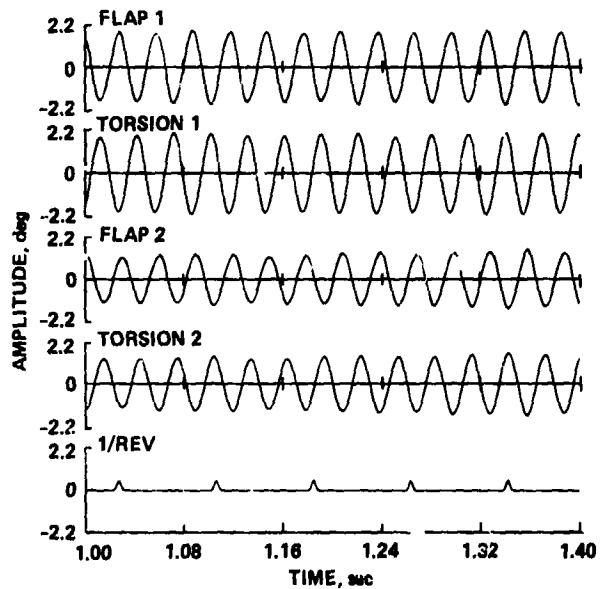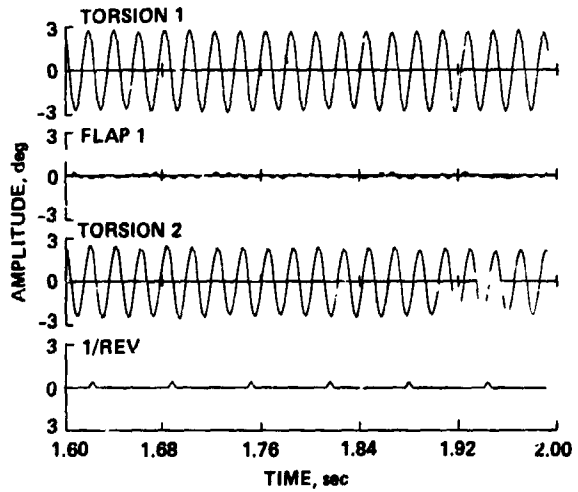
(a) Time-history.
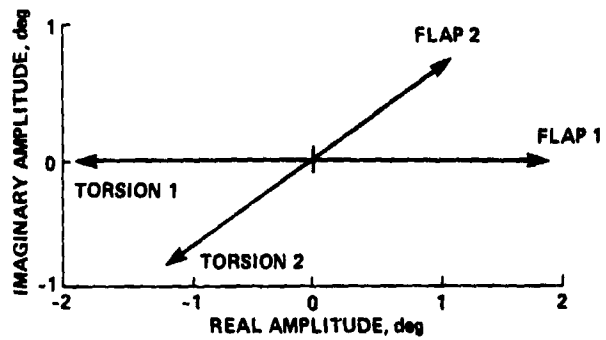
(b) Vector phase plot, $\omega = 33.55$ Hz.

Figure 5. Time-history and vector phase plot for Type 1 flutter [(2c)]; two blades, $\theta = 0°$, $\Omega = 762$ rpm.

82
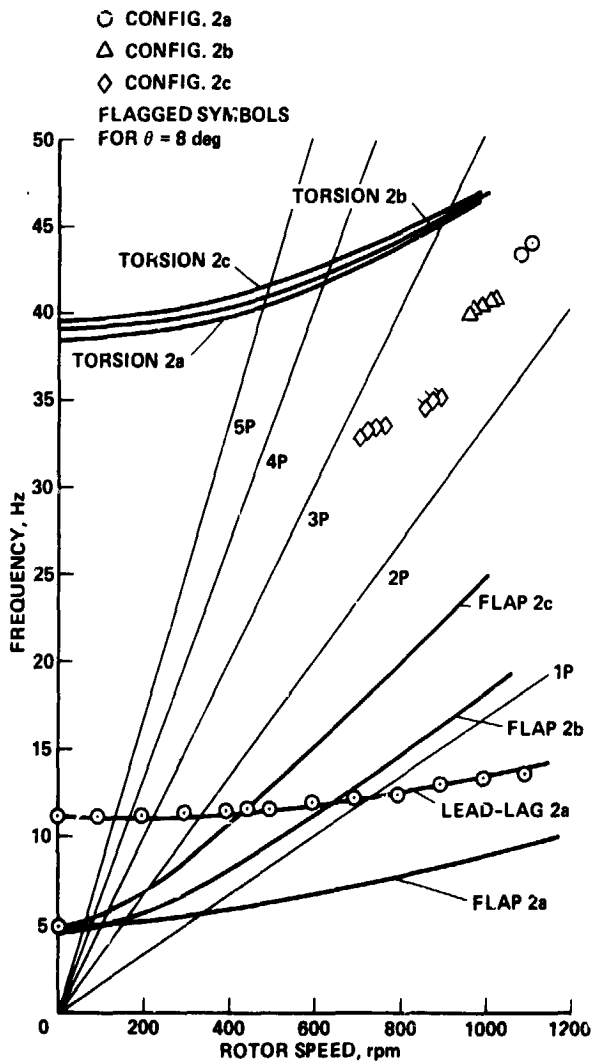
Figure 6. Frequency diagram for Type 1 flutter [(2a), (2b), and (2c)]. (Flagged symbols are for θ = 8°).
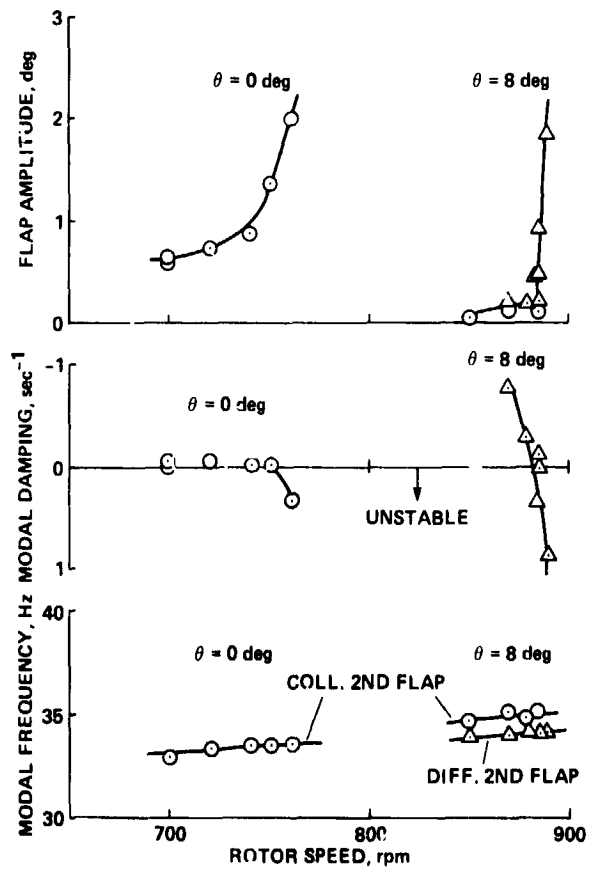
Figure 7. Type 1 flutter behavior for (2c).
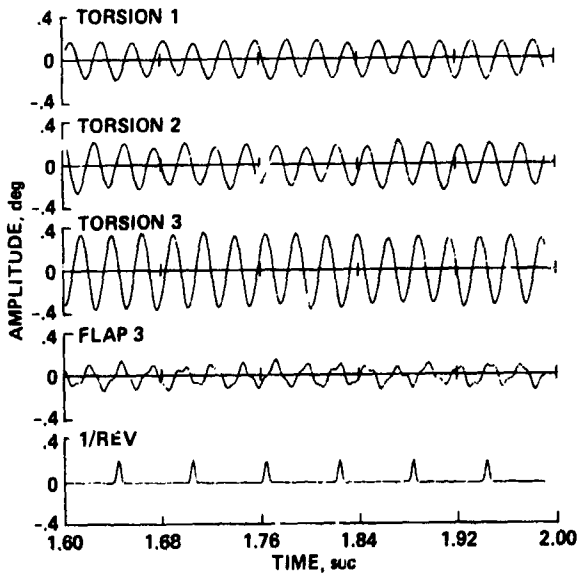
(a) Time-history.
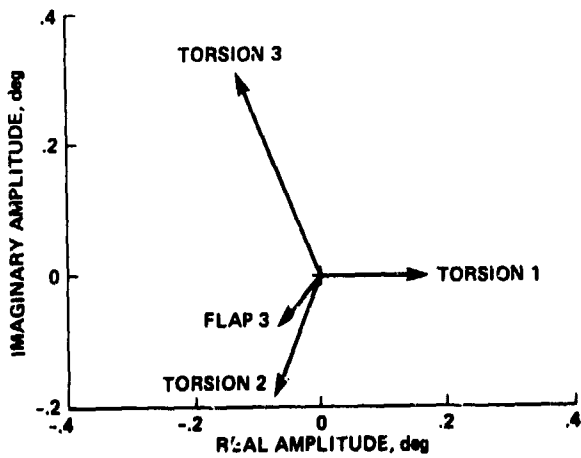
(b) Vector phase plot, ω = 39.92 rpm.

Figure 8. Time-history and vector phase plot for Type 1 flutter [(17a)]; three blades, θ = 0°, Ω = 999 rpm.

(a) Time-history.
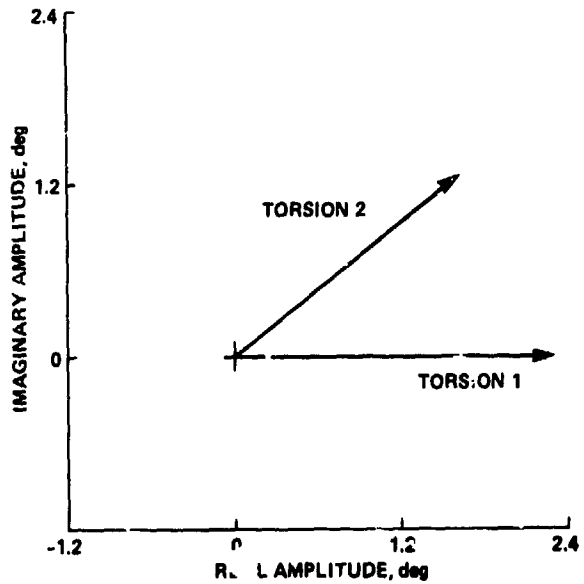
(b) Vector phase plot, ω = 48.82 Hz.

Figure 9. Time-history and vector phase plot for Type 2 flutter [(3a)]; two blades, θ = 0°, Ω = 936 rpm.
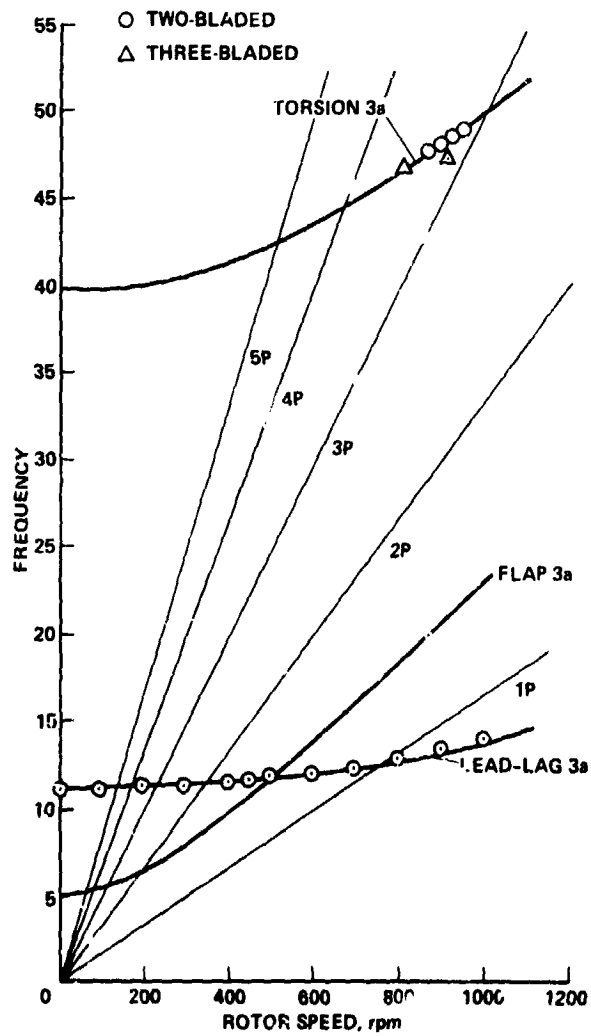
Figure 10. Frequency diagram for Type 2 flutter [(3a)].
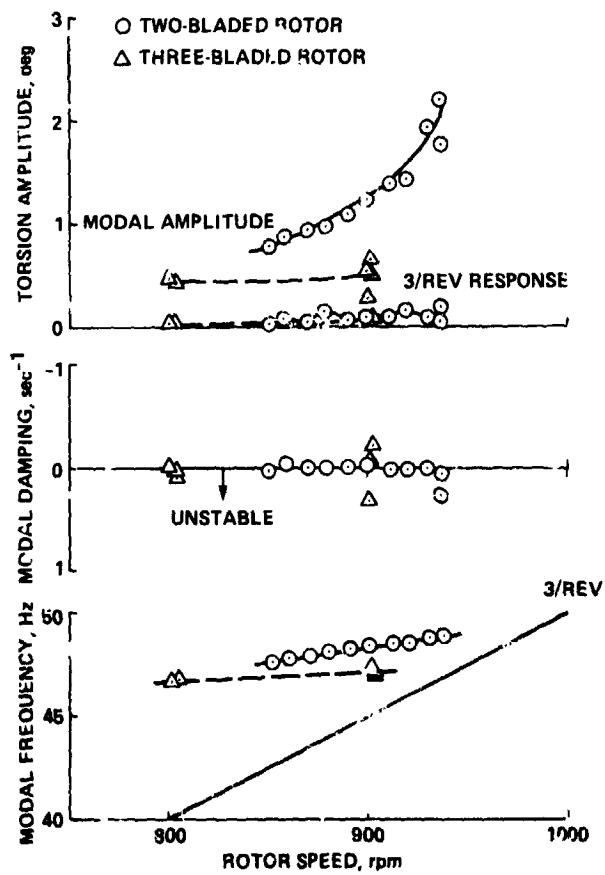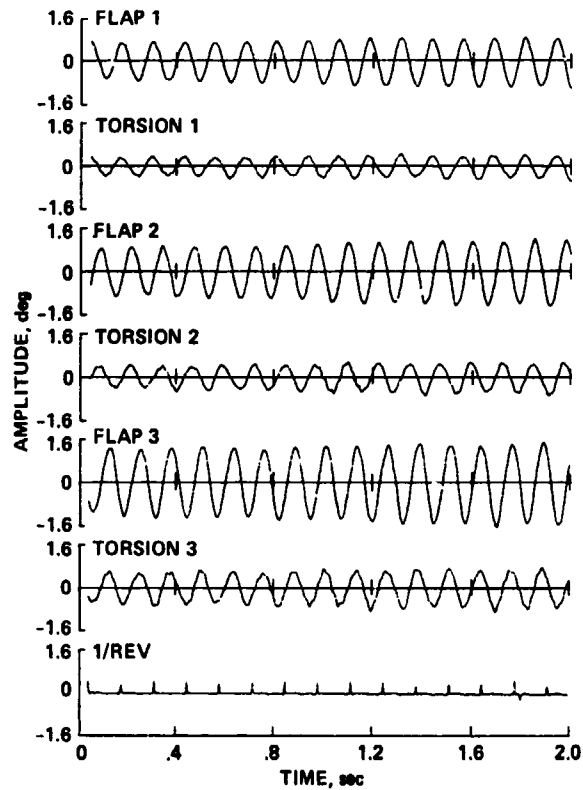
Figure 11. Type 2 flutter behavior for (3a).
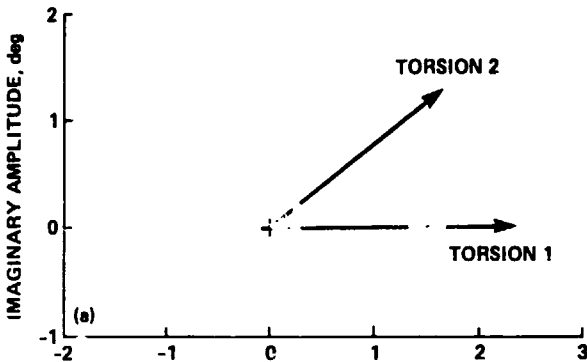
(a) Two-bladed rotor, $\Omega = 936$ rpm, $\omega = 48.82$ Hz.
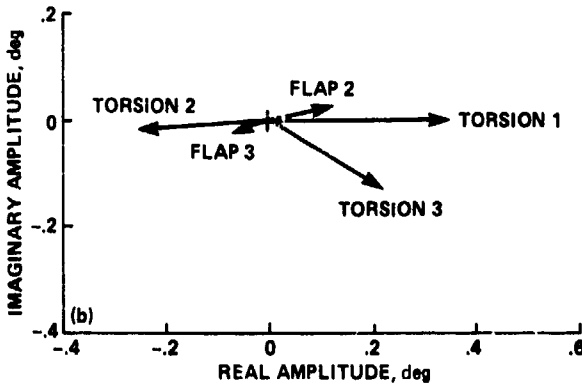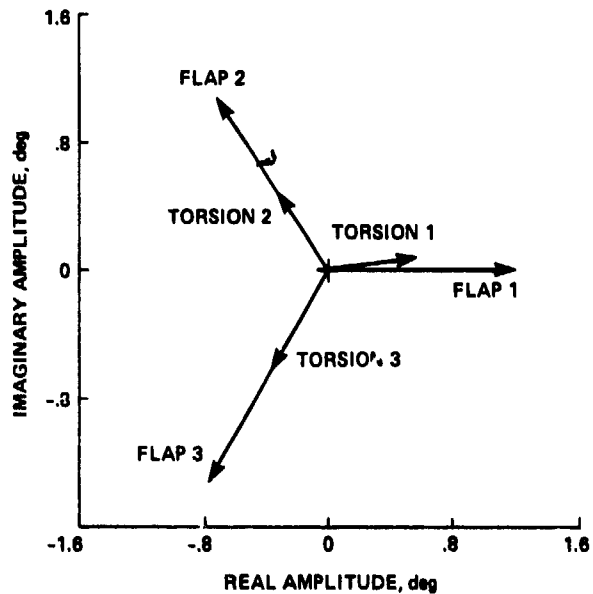

(b) Three-bladed rotor, $\Omega = 900$ rpm, $\omega = 47.33$ Hz.

Figure 12. Comparison of vector phase plots for two- and three-bladed rotors for (3a); $\theta = 0°$.

(a) Time-history.

(b) Vector phase plot, $\omega = 7.94$ Hz.

Figure 13. Time-history and vector phase plot for Type 3 flutter [(15a)]; three blades, $\theta = 0°$, $\Omega = 451$ rpm.
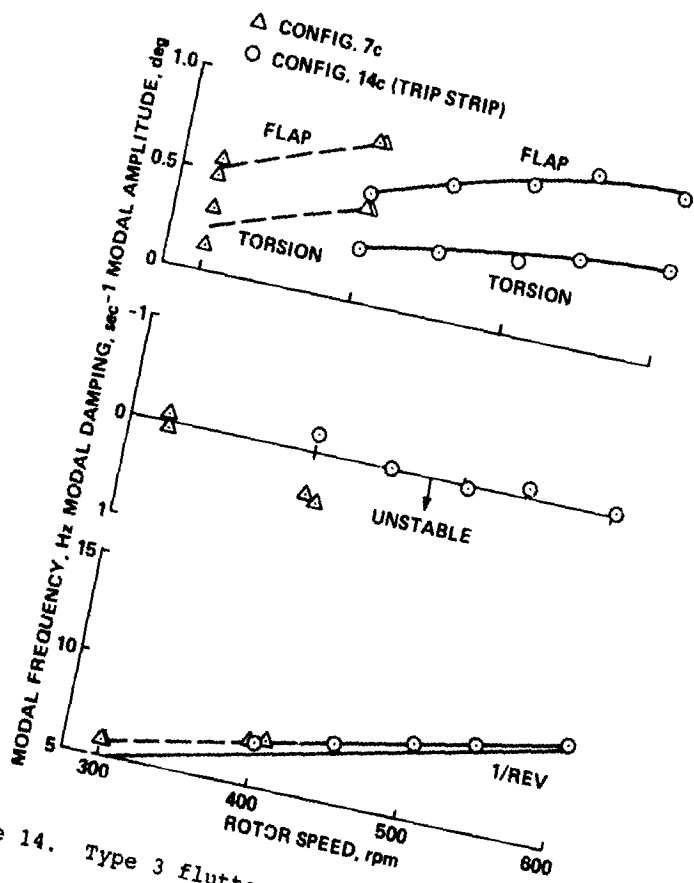
86

C - 2

Figure 14. Type 3 flutter behavior for (7c and 14c).

DISCUSSION
Paper No. 6

EXPERIMENTALLY DETERMINED FLUTTER FROM TWO- AND THREE-BLADED MODEL
BEARINGLESS ROTORS IN HOVER
William G. Bousman
and
Seth Dawson

Jing Yen, Bell Helicopter: Is where any way we can look at these mode shapes. For the Type 1 you have is the mode a predominantly beamwise mode and is Type 2 predominantly a torsion mode?

Bousman: Type 1 for almost all cases had roughly comparable motions in flapping and torsion. I would say it was a mixture of second flap and first torsion mode behavior. It's fairly near that crossing.

Yen: It looks like the frequency is a strong function of rpm.

Bousman: Yes. That frequency is occurring, as best we can tell, at the second flap mode, although we don't have any calculations, because FLAIR doesn't do calculations of higher modes.

Yen: My second question, Bill, do you still have the model parts around the lab? Can you put them back together again, run up and blow some wind?

Bousman: Blow some wind?

Yen: Yes. In other words could this be a wake flutter?

Bousman: Oh, you mean particularly for the one that we think is a wake flutter. Could we blow some wind and just see if it goes away. Yes, that's a good idea.